

Unsupervised Deep Context Prediction for Background Estimation and Foreground Segmentation

Maryam Sultana · Arif Mahmood · Sajid Javed · Soon Ki Jung

Received: date / Accepted: date

Abstract In many high level vision applications such as tracking and surveillance, background estimation is a fundamental step. In the past, background estimation was usually based on low level hand-crafted features such as raw color components, gradients, or local binary patterns. These existing algorithms observe performance degradation in the presence of various challenges such as dynamic backgrounds, photo-metric variations, camera jitter, and shadows. To handle these challenges for the purpose of accurate background estimation, we propose a unified method based on Generative Adversarial Network (GAN) and image inpainting. It is an unsupervised visual feature learning hybrid GAN based on context prediction. It is followed by a semantic inpainting network for texture optimization. We also propose a solution of arbitrary region inpainting by using center region inpainting and Poisson blending. The proposed algorithm is compared with the existing algorithms for background estimation on SBM.net dataset and for foreground segmentation on

CDnet 2014 dataset. The proposed algorithm has outperformed the compared methods with significant margin.

Keywords Background subtraction · Foreground detection · Context-prediction · Generative Adversarial Networks

1 Introduction

Background estimation and foreground segmentation is a fundamental step in several computer vision applications, such as salient motion detection [13], video surveillance [3], visual object tracking [51] and moving objects detection [41, 34, 14]. The goal of background modeling is to efficiently and accurately extract a model which describes the scene in the absence of any foreground objects. Background modeling becomes challenging in the presence of dynamic backgrounds, sudden illumination variations, and camera jitter which is mainly induced by the sensor. A number of techniques have been proposed in the literature that mostly address relatively simple scenarios for scene background modeling [4], because complex background modeling is a challenging task itself specifically in handling real-time environments.

To solve the problem of background subtraction, Stauffer *et al.* [39] and Elgammal *et al.* [11] presented methods based on statistical background modeling. It starts from an unreliable background model which identify and correct initial errors during the background updating stage by the analysis of the extracted foreground objects from the video sequences. Other methods proposed over the past few years also solved background initialization as an optimal labeling problem [29, 31,

Maryam Sultana, Soon Ki Jung
School of Computer Science and Engineering
Virtual Reality Laboratory,
Kyungpook National University,
Daegu, Republic of Korea,
E-mail: maryam@vr.knu.ac.kr, skjung@knu.ac.kr

Arif Mahmood
Department of Computer Science and Engineering
Qatar University
Doha, Qatar
E-mail: rfmahmood@gmail.com

Sajid Javed
Department of Computer Science
Tissue Image Analytics Laboratory
University of Warwick
United Kingdom,
E-mail: s.javed.1@warwick.ac.uk

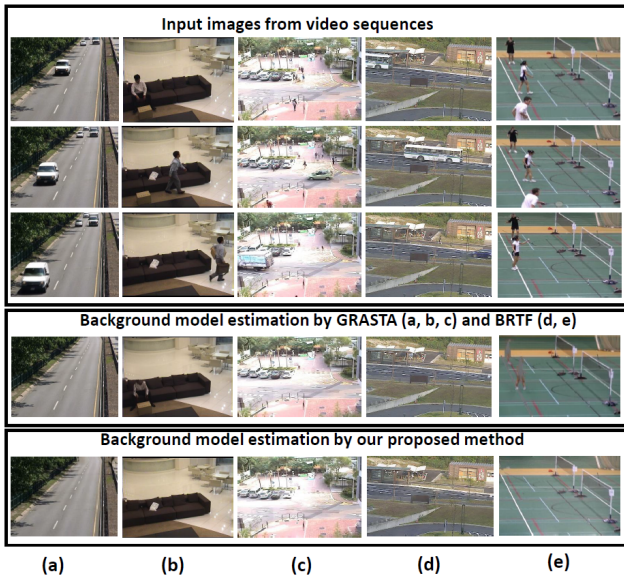


Fig. 1 Estimated background images from the SBM.net dataset : Sequences in (a) are from the category "Basic" named "Highway". (b) Sequence "Sofa" from the category "Intermittent Object Motion" (c) Sequence "Chuk Square" from the category "Very Short". (d) Sequence "Bus Station" from the category "Very Long". (e) Sequence "Badminton" is also from the category "Jitter". In almost all of these cases, for accurate the background estimation, the average gray-level error (AGE) is less in our proposed algorithm as mentioned in Table 1.

47]. These methods compute label for each image region, provide the number of the best bootstrap sequence frame such that the region contains background scene. Taking into account spatio-temporal information, the best frame is selected by minimizing a cost function. The background information contained in the selected frames for each region is then combined to generate the background model. The background model initialization methods based on missing data reconstruction have also been proposed [38]. These methods work where missing data are due to foreground objects that occlude the bootstrap sequence. Thus, robust matrix and tensor completion algorithms [37] as well as inpainting methods [9] have shown to be suitable for background initialization. More recently, deep neural networks are introduced for image inpainting [32]. In particular, Chao Yang et al. [48] used a trained CNN (Context Encoder [32]) with combined reconstruction loss and adversarial loss [15] to directly estimate missing image regions. Then a joint optimization framework updates the estimated inpainted region with fine texture details. This is done by hallucinating the missing image regions via modeling two kinds of constraints, the global context based and the local texture based, with convolutional neural networks. This framework is able to estimate missing image structure, and is very fast to evaluate.

Although the results are encouraging but it is unable to handle random region inpainting task with fine details.

In this paper we propose to predict missing image structure using inpainting method, for the purpose of scene background initialization. We name our method as *Deep Context Prediction* (DCP), because it has the ability to predict context of a missing region via deep neural networks. Few visual results of the proposed DCP algorithm are shown in Figure 1. Given an image, fast moving foreground objects are removed using motion information leaving behind missing image regions (see Figure 2 Step (1)). We train a convolutional neural network to estimate the missing pixel values via inpainting method. The CNN model consists of an encoder capturing the context of the whole image into a latent feature representation and a decoder which uses this representation to produce the missing content of the image. The model is closely related to auto-encoders [2, 19], as it shares a similar architecture of encoder-decoder. Our contributions in the proposed method are summarized as follows:

- We extract the temporal information in the video frames by using dense optical flow [26]. After mapping motion information to motion mask, we are able to approximately identify fast moving foreground objects. We eliminate these objects and fill the missing region using the proposed DCP algorithm by estimating background.
- In our proposed DCP method, we train a context encoder similar to [48] on scene-specific data. The network is pre-trained on ImageNet dataset [10]. DCP is a joint optimization framework that can estimate context of missing regions by inpainting in central shape and later transform this predicted information to random regions by the help of Modified Poisson Blending (MPB) [1] technique. The framework is based on two constraints, a global context based which is a hybrid GAN model trained on scene-specific data and a local texture based which is VGG-19 network [36].
- For the purpose of foreground object detection, we first estimate background via DCP, and later we binarize the difference of the background with the current frame, leading to more precise detection of foreground moving objects. This binarized difference is enhanced through morphological operations to remove false detection and noisy pixel values.

The proposed DCP algorithm is based on context prediction, therefore it can predict homogeneous or blurry contexts more accurately compared to other background initialization algorithms. In case of background motion,

DCP can still estimate background by calculating motion masks via optical flow, as our target is to eliminate foreground moving objects only. DCP is also not effected by intermittent object motion because of the same reason mentioned previously. In challenging weather conditions (rain, snow, fog) dense optical flow can identify foreground moving objects, so targeting only those objects to remove and inpaint them with background pixels makes DCP a good background estimator. For the case of difficult light conditions DCP can estimate background accurately because of homogeneity in the context of scenes with low illumination.

2 Related Work

Over the past few years, background subtraction and foreground detection has remained the part of many key research studies [7, 30, 17, 21, 20] as well as scene background initialization [4, 3, 12, 28, 49]. In the problem of background subtraction, the critical step is to improve the accuracy of the detection of foreground. On the other hand, the task of estimating an image without any foreground is called scene background modeling. Many comprehensive studies have been conducted to this problem [4, 3, 28]. Gaussian Mixture Model (GMM) [39, 50, 56, 40, 27] is a well known technique for background modeling. It uses probability density functions as mixture of Gaussians to model color intensity variations at pixel level. Recent advances in GMM include minimum spanning tree [8] and bidirectional analysis [35]. On the other hand most GMM based methods also suffer performance degradation in complex and dynamic scenes.

In the past, particularly for the problem of background modeling many research studies have been conducted by using *Robust Principal Component Analysis* (RPCA). Wright *et al.* [44] presented the first proposal of RPCA-based method which has the ability to handle the outliers in the input data. Later Candes *et al.* [6] used RPCA for background modeling and foreground detection. Beyond good performance, RPCA-based methods are not ideal for real-time applications because these techniques possess high computational complexity. Moreover, conventional RPCA-based methods process data in batch manner. Batch methods are not suitable for real-time applications and mostly work offline. Some online and hybrid RPCA based methods have also been presented in the literature to handle the batch problem [22] while global optimization is still a challenge in these approaches [20, 18, 46]. Xiaowei Zhou *et al.* [55] proposed an interesting technique known as *Detecting Contiguous Outliers in the LOW-rank Representation* (DECOLOR). Limitation of no prior knowl-

edge in RPCA based methods on the spatial distribution of outliers leads to develop this technique. Outliers information is modeled in this formulation by using Markov Random Fields (MRFs). Another online RPCA algorithm proposed by Jun He *et al.* [18] is *Grassmannian Robust Adaptive Subspace Tracking Algorithm* (GRASTA). It is an online robust subspace tracking algorithm embedded with traditional RPCA. This algorithm operates on data which is highly sub-sampled. If the observed data matrix is corrupted by outliers as in most cases of real-time applications, l^2 -norm based objective function is best-fit to the subspace. Hybrid Approach: use a time window to obtain sufficient context information then process it like a small batch. Recently S. Javed *et al.* [23] proposed a hybrid technique named *Motion-assisted Spatiotemporal Clustering of Low-rank* (MSCL) based on RPCA approach. In this method for each data matrix, sparse coding is applied and estimation of the geodesic subspace based Laplacian matrix is calculated. The normalized Laplacian matrices estimated over both distances Euclidean as well as Geodesic are embedded into the basic RPCA framework. In 2015 Liu *et al.* [54] developed a technique called *Sparse Matrix Decomposition* (SS-GoDec), which is capable of efficiently and robustly estimating the low-rank part L of background and the sparse part S of an input data matrix $D = L + S + G$ with a factor of noise G . This technique alternatively assigns the low-rank approximation of difference between input data matrix and sparse matrix ($D - S$) to L . Similarly it also assigns the vice versa as well which is the sparse approximation of ($D - L$) to S . To overcome the batch constraint of RPCA based methods J. Xu *et al.* [45] presented a method called *Grassmannian Online Subspace Updates with Structured-sparsity* (GOSUS). Although this method performs well for background estimation problem but global optimality is still the challenging issue in this approach. Qibin Zhao *et al.* [53] presented a method called *Bayesian Robust Tensor Factorization for Incomplete Multiway Data* (BRTF). This method is a generative model for robust tensor factorization in the presence of missing data and outliers. X. Guo *et al.* [16] presented a method called *Robust Foreground Detection Using Smoothness and Arbitrariness Constraints* (RFSA). In this method the authors considered the smoothness and the arbitrariness of static background, thus formulating the problem in a unified framework from a probabilistic perspective.

Recently, Convolutional Neural Network (CNN) based methods have also shown significant performance for foreground detection by scene background modeling [5, 43, 52]. For instance, Wang *et al.* [43] proposed a simple yet effective supervised CNN based method for detect-

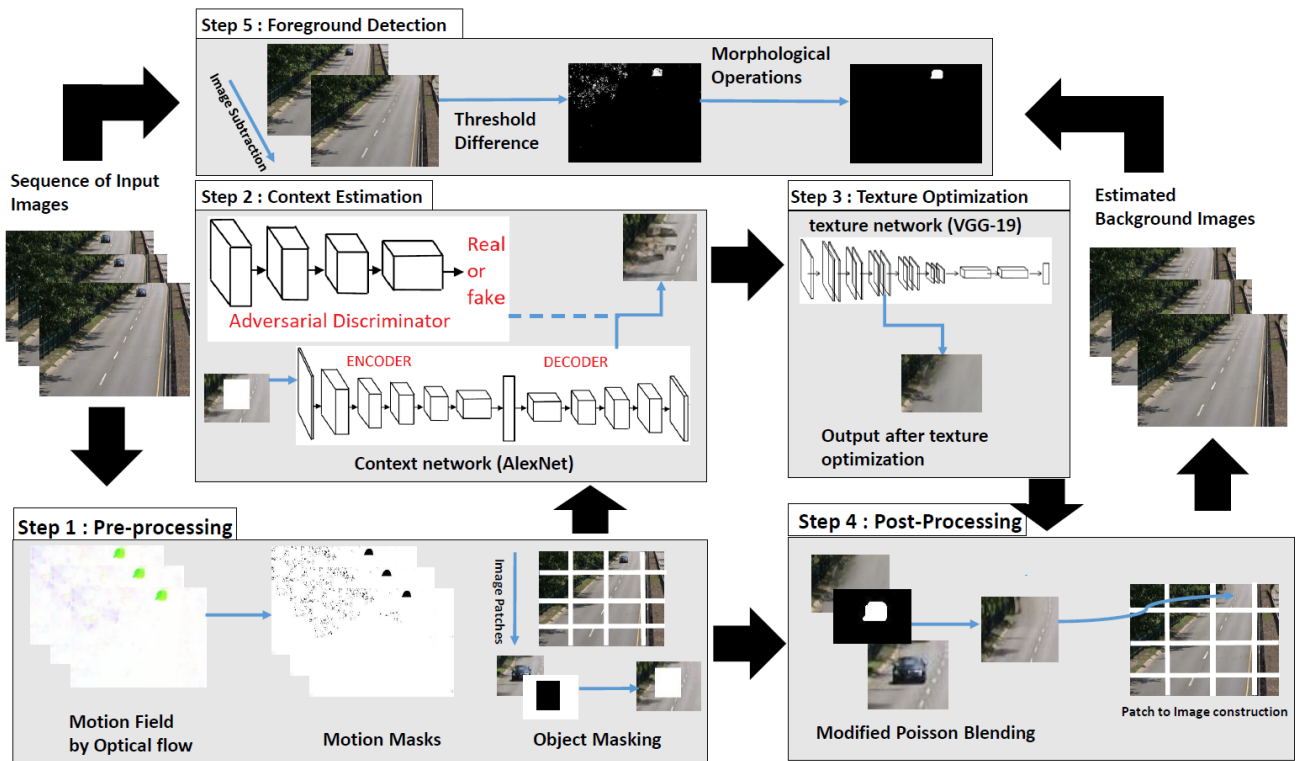


Fig. 2 Workflow of the proposed algorithm for background estimation. Step (1) describes the motion estimation via dense optical flow, the creation of motion masks, image to patch conversion and object masking for center region inpainting task. Step (2) evaluates the prediction of missing region with context prediction hybrid GAN network. In step (3), to improve the fine texture details of the predicted context, the output of step (2) is given to texture network. Step (4) In the previous step it can be seen that in this case some information of road (white lines in the middle) is being missed by texture network so, Modified Poisson Blending technique is applied to get final results. Step (5) we threshold the difference of the estimated background via DCP and current frame of the video sequence. Afterwards the thresholded difference is binarized and run through extensive Morphological Operations to extract the foreground moving object.

ing moving objects in static background scenes. CNN based methods perform best in many complex scenes however, our proposed method DCP is unsupervised therefore it do not require any labelled data for training purposes.

3 Proposed Method

Our proposed background foreground separation technique has five steps. 1.) Motion masks evaluation via dense optical flow. 2.) Estimation of missing background pixels by Context Encoder (CE). 3.) The improvement of estimated missing pixels texture by a multi-scale neural patch synthesis. 4.) Modified Poisson Blending technique is applied to get final results. 5.) The foreground objects are detected by applying threshold on the difference between the estimated background from DCP and the current frame, which is later enhanced by morphological operations. The work flow diagram of DCP is shown in Figure 2. Detail description of the above mentioned steps is as follows:

3.1 Motion Masks via Optical Flow

For the purpose of background estimation from the video frames, we have to first identify the fast moving foreground objects. These objects are recognized by using optical flow [26] which is then used to create a motion mask. Dense optical flow is calculated between each pair of consecutive frames in the given input video sequence S . Motion mask M is computed by using motion information from a sequence of video frames. Let S_t and S_{t-1} be the two consecutive frames in S at time instant t and $t-1$, respectively. Considering $v_{t,p}^y$ be the vertical component and $u_{t,p}^x$ be the horizontal component of the motion vector at position p which is computed between consecutive frames. The corresponding motion mask, $m_t \in \{0, 1\}$ will be computed as :

$$m_{t,p} = \begin{cases} 1, & \text{if } \sqrt{(u_{t,p}^x)^2 + (v_{t,p}^y)^2} < t_h, \\ 0, & \text{otherwise.} \end{cases} \quad (1)$$

In the above equation, t_h is threshold of motion magnitude. It is computed by taking the average of all pix-

els in the motion field. Selection of the threshold t_h is adapted in such a way that all pixels in S consisting of motion greater than t_h belongs to the foreground. In order to avoid noise in the background, threshold t_h is selected to be large enough.

3.2 Background Pixels Estimation via Context Prediction

Given image patches from a video with missing regions such as foreground object regions, we predict context via context encoder [32]. The context encoder is a hybrid GAN model which is trained on the basis of convolutional neural network to estimate the missing pixel values. It consists of two parts: an encoder which captures the context of a given image patch into a compact latent feature space. While the other part is a decoder which uses encoded representation to produce missing image patch content. Overall architecture of context encoder is a simple encoder-decoder pipeline.

The encoder is derived from the AlexNet [24], however the network is not trained for classification, rather it is trained for context prediction. Training is performed on ImageNet as well as using scene-specific video sequences patches. In order to learn an initial context prediction network, we train a regression network F to get response $F(x_m)$, where x_m is the input image patch x pixel-wise multiplied by object mask m_o : $x_m = x \odot m_o$. Since m_o is a binary mask with fix central region which covers the whole object in motion mask.

The patch x_m with a missing region H , is input to Context Network. The response $F(x_m)$ of trained context network is estimated via joint loss functions to estimate the background x_b in the missing region H . We have experimented with two joint loss functions including reconstruction loss L_{rec} and adversarial loss L_{adv} [32]. The reconstruction loss L_{rec} is defined as:

$$L_{rec}(x_m, x_b, H) = \|F(x_m) - C(x_b, H)\|_2^2. \quad (2)$$

The adversarial loss is given as:

$$L_{adv}(x_m, x_b, H) = \max_D E_{x_m \in \chi_m} [\log(D(C(x_b, H))) + \log(1 - D(F(x_m)))], \quad (3)$$

where D is the adversarial discriminator and $C(\cdot)$ defines the operation of extracting a sub-image in the central region during inpainting process. Overall loss function is a linear combination of both reconstruction and adversarial losses.

$$L = \eta L_{rec}(x_m, x_b, H) + (1 - \eta) L_{adv}(x_m, x_b, H), \quad (4)$$

where η is a relative weight of each loss function.

3.3 Texture Optimization of Estimated Background

In the last section, we estimated a background patch x_b via Context Encoder (CE). But the estimated context still contains irregularities and blurry texture at low resolution of the image patch. To solve this blurry estimated context problem for high resolution inpainting with fine details, we use texture network at three-level pyramid of image patches. This network optimizes over three loss terms: the predicted context term initialized by CE, the local texture optimization term, and the gradient loss term. The context prediction term captures the semantics including global structures of the image patches. The texture term maps the local statistics of input image patch texture, and the gradient loss term enforces the smoothness between the estimated context and the original context. For three-level pyramid approach the test image patch is assumed to be always cropped to 512×512 with a 256×256 hole in the center at fine level. However with step-size two, downsizing to the coarse level as 128×128 size image patch with a 64×64 missing region is initialized by CE. Afterwards context of missing region is estimated in a coarse-to-fine manner. At each scale, the joint optimization is performed to update the missing region and then upsampling is done to initialize the joint optimization which sets the context constraint for the next scale of image patch. This process repeats this until the joint optimization is completed at the fine level of the pyramid. The texture optimization term is computed using the *VGG-19* [36] which is pre-trained on ImageNet.

Once the context is initialized by CE at the coarse scale, we use the output $F(x_m)$ and the original image as the initial context constraint for joint optimization. Let x_o be the original image patch with missing region filled with the CE. Upsampled version of x_o are used as the initialization for joint optimization at the fine scales.

For the input image patch x_o we would like to estimate the fine texture of the missing region. The region corresponding to x_o in the feature map of *VGG-19* network is $\psi(x_o)$ and $\psi(H)$ is the feature map corresponding to the missing region. For texture optimization $C(\cdot)$ also defines the operation of extracting a sub-feature-map in a rectangular region, i.e. the context of $\psi(x_o)$ within $\psi(H)$ is returned by $C(\psi(x_o), H)$.

The optimal solution for accurate reconstruction of the missing content is obtained by minimizing the following objective function at each scale $i = 1, 2, \dots, n$.

$$\hat{x}^{i+1} = \arg \min E_{CE}(C(x_o, H), C(x_o^i, H)) + \gamma E_T(\psi_T(x_o), \psi(H) + \delta \Pi(x_o)), \quad (5)$$

where $C(x_o^1, H) = F(x_o)$, $\psi_T(\cdot)$ represents a feature maps in the texture network T at an intermediate layer, γ and δ are weighting reflecting parameters. [48]. The first term E_{CE} in equation (5) is context constraint which is defined by the difference between the previous context prediction and the optimization result:

$$E_{CE}(C(x_o, H), C(x_o^i, H)) = \|C(x_o, H) - C(x_o^i, H)\|_2^2. \quad (6)$$

The second term E_T in equation (5) handles the local texture constraint, which minimizes the inconsistency of the texture appearance outside and inside the missing region. We first select a single feature layer or a combination of different feature layers in the texture network T , and then extract its feature map ψ_T . In order to do texture optimization, for each query local patch P of size $w \times w \times c$ in the missing region $\psi(H)$, our target is to find the most similar patch outside the missing region, and calculate loss as mean of the query local patch and its nearest neighbor distances.

$$E_T(\psi_T(x_o), H) = \frac{1}{|\psi(H)|} \sum_{i \in \psi(H)} \|C(\psi_T(x_o), P_i) - C(\psi_T(x_o), P_{np(i)})\|_2^2, \quad (7)$$

In the above equation, the local neural patch centered at location i is P_i , the number of patches sampled in the region $\psi(H)$ is given by $|\psi(H)|$, and $np(i)$ is the calculated as:

$$np_i = \arg \min_{j \in n(i) \wedge j \notin H^\psi} \|C(\psi_T(x), P_i) - C(\psi_T(x), P_j)\|_2^2, \quad (8)$$

where $n(i)$ is the set of neighboring locations of i excluding the overlap with the missing unknown region $\psi(H)$. We also add the gradient loss term to encourage smoothness in texture optimization [48]:

$$\Pi(x_o) = \sum_{j,k} ((x_o(j, k+1) - x_o(j, k))^2 + (x_o(j+1, k) - x_o(j, k))^2), \quad (9)$$

3.4 Blending of Estimated and Original Textures

After the texture optimization, some information around the central region during inpainting process is being missed or removed due to rectangular shaped region as shown in figure 2. In order to change the rectangular shaped predicted context to the irregular shaped region, Modified Poisson Blending technique (MPB) [1]

is used. It is based on Poisson image editing for the purpose of seamless cloning. The MPB technique has three steps, the first step, uses the source image which is inpainted image via DCP as a known region and the target image which is original image containing foreground as an unknown region. Afterwards it requires motion mask by optical flow around the interested object in the source image for solving Poisson equation [33] under gradient field and predefined boundary condition. MPB technique has few modifications to Poisson image editing technique that eliminates the bleeding problems in the composite image by using Poisson blending with fair dependency of source which is inpainted context and target pixels which are original image pixels. In the next step, MPB technique uses the composite image as unknown region and the target image with foreground object as a known region. After applying Poisson blending algorithm, we get another composite image which will be used in third step. To reduce bleeding artifacts, MPB technique generate an alpha mask that is used to combine both composite images from previous steps to get final image that is free from color bleeding. In practice this method helps in discarding the useless information which came along rectangular region inpainting process.

3.5 Foreground Detection

In this work we mainly focus on the problem of background initialization. However, in this section we extend our work to foreground detection as well. Thus we are able to compare our work with foreground detection algorithms as well, in addition to the work on background initialization only. For the purpose of foreground detection, we threshold the difference of the estimated background via DCP and the current frame of the video sequence. The difference is threshold and binarized and processed through Morphological Operations (MO) with suitable Structuring Elements (SE). Thus the work done in this section may be considered as post processing.

These operations first include opening operation of an image which is erosion followed by the dilation with the same SE:

$$I \circ SE = (I \ominus SE) \oplus SE, \quad (10)$$

where I is the binarized difference, \ominus and \oplus denote erosion and dilation respectively. Afterwards, closing operation is performed on this image. It is in reverse way, that is dilation followed by erosion with same SE, but different from SE used in the opening operation.

$$I' \bullet SE = (I' \oplus SE) \ominus SE. \quad (11)$$

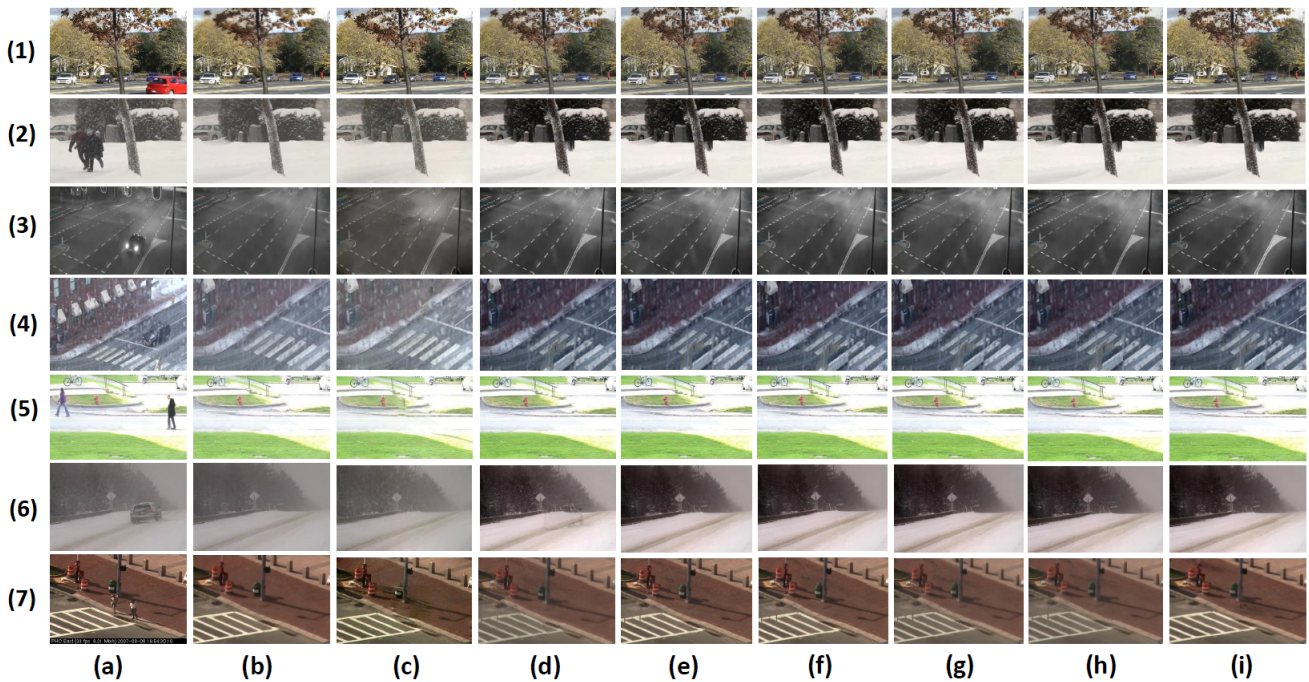


Fig. 3 Qualitative results of the proposed method. (a) 7 images from the input video sequences, (b) Ground truth, (c) estimated background model by the proposed DCP method, (d) RFSA, (e) GRASTA, (f) BRTF, (g) GOSUS, (h) SSGoDec, (i) DECOLOR. From top to bottom: each input sequence is selected from different categories. (1) sequence "Fall" from "Background Motion", (2) "Skating" from "Basic", (3) "StreetCornerAtNight" from "Basic", (4) "WetSnow" from "Basic", (5) "Pedestrians" from "Very Short", (6) "Snowfall" from "Very Short", and (7) "SideWalk" from "Jitter".

Now here I' is the difference image from equation (10), \oplus and \ominus denote dilation and erosion respectively. Successive opening and closing of the binarized difference frame with proper SE leads us to separate the foreground objects from the background. The choice of the SE is very crucial in successive opening and closing of the binarized difference frame as it may lead to false detection if not selected according to the shape of the objects in the video frames. The MO not only fills the missing regions in thresholded difference but also removes the unconnected pixels values of background which are considered to be noise in foreground detection process.

4 Experiments

Our background estimation and foreground detection techniques are based on inpainting model similar to [48]. We trained the context prediction model additionally with scene-specific data in terms of patches of size 128×128 for 3 epoches. The texture optimization is done with *VGG-19* network pre-trained on ImageNet for classification. The frame selection for inpainting the background is done by summation of pixel values in the forward frame difference technique. If the sum of difference pixels is small, then current frame is selected.

We evaluate our proposed approach on two difference datasets, including Scene Background Modeling (SBM.net)¹ for background estimation and Change Detection 2014 Dataset (CDnet2014)[42] for foreground detection. On both datasets our proposed algorithm has outperformed existing state of the art algorithms with a significant margin.

4.1 Evaluation of Deep Context Prediction (DCP) for Background Estimation

We have selected all videos out of 7 categories from SBM.net dataset as shown in Table 1. Every category in SBM.net dataset has challenging video sequences for background modeling. In this experiment, results are compared with 6 state-of-the-art methods, including RFSA [16], GRASTA [18], BRTF [53], GOSUS [45], SSGoDec [54], and DECOLOR [55] using implementations of the original authors. Background estimation models are compared using Average Gray-level Error (AGE), percentage of Error Pixels (pEPs), Percentage of Clustered Error Pixels (pCEPs), Multi Scale Structural Similarity Index (MSSSIM), Color image Quality Measure (CQM), and Peak-Signal-to-Noise-Ratio (PSNR)

¹ <http://scenebackgroundmodeling.net/>

[28]. For best performance the aim is to minimize AGE, pEPs, and pCEPs while maximizing MSSSIM, PSNR, and CQM (Fig. 5). The detail description of results with respect to each category is as follows:

Category: Background Motion contains 6 video sequences. In this category the proposed DCP algorithm achieved best performance among all the compared methods. The performance of DECOLOR, SSGoDec, RFSA, GRASTA and BRTF has remained quite similar with minimal difference in AGE as shown in table 1. GOSUS has the highest average gray level error among all the compared methods. Targeting only foreground objects to be eliminated and filled with background pixel values via inpainting method makes DCP to perform better in this category as compared to all other methods. The visual results are shown in Figure 3, 1st row.

Category: Basic contains 16 video sequences (Table 1). In almost all video sequences our proposed approach DCP performed well. DCP achieved an average AGE of 5.367 (visual results in Figure 4) among all the compared methods because this category contains relatively simple scenes for background estimation. It can be seen in the Table 1, that RFSA, BRTF and DECOLOR almost achieved equal and second lowest score of AGE but GOSUS and GRASTA achieved a bit higher values of AGE. GOSUS suffered performance degradation among all compared methods. In terms of qualitative analysis DCP estimated better background as compared to all the methods, results are shown in the Figure 3, (c), (d) and (e). The reason is that the context for video sequences of ‘Wet-snow’, ‘Skating’ and ‘Street Corner at Night’ is homogeneous in the whole frame as background pixel values. This key aspect is favorable for our proposed method.

Category: Intermittent Motion contains 16 video sequences (Table 1). This category has video sequences which contain ghosting artifacts in the detected motion. DCP performed well in this category by achieving lowest AGE score of 9.344 among all compared techniques. Methods including RFSA, GRASTA, BRTF, GOSUS and SSGoDec achieved almost equal and higher score of AGE (Figure 4 and Table 1). DECOLOR has the highest error rate in background estimation for this category. The ghosting artifacts pose big challenge for all algorithms as the foreground becomes the part of background, resulting in failure of accurate background recovery model.

Category: Jitter contains 9 video sequences (Table 1). DCP achieved lowest average gray level error among all the compared methods due to the fact that camera jitter contains videos sequences with blurry context and such context is easy to predict by our proposed

method. RFSA, BRTF and GOSUS achieved higher AGE score in this category while GRASTA and DECOLOR showed performance degradation among all compared methods. It can be seen in Figure 1 (e) that GRASTA was not able to recover clean background while DCP estimated it accurately. SSGoDec is also able to recover clean background as shown in Figure 3 (h) with low AGE score.

Category: Very Short contains 10 video sequences each having only few frames (Table 1). DCP achieved the lowest AGE score in this category too. GOSUS also performed well and achieved the second lowest AGE score as shown in Table 1. However RFSA, GRASTA, BRTF, DECOLOR and SSGoDec achieved almost equal score of AGE among all the compared methods. In terms of qualitative analysis, it can be seen in Figure 3 (c) that for instance, the video sequence ‘SnowFall’, DCP achieved the lowest score of AGE. It is due to the fact that in case of bad weather snow or rain the context of the videos gets blurry which is rather easy for DCP to estimate.

Category: Illumination Changes contains 6 video sequences (Table 1). This category pose a great deal of challenge for all the methods. DCP managed to get lowest AGE score among all the compared methods due to the fact that context prediction in low light and with less sharp details is rather favorable condition for our proposed method. GRASTA, GOSUS and SSGoDec also performed well and achieved second lowest AGE score among all compared methods. BRTF and DECOLOR almost get equal AGE score. RFSA has the highest error rate as shown in Table 1, because of the spatio-temporal smoothness of foreground, and the correlation of background constraint.

Category: Very Long contains 5 video sequences containing thousands of frames (Table 1). Among all the compared methods only DCP and DECOLOR performed well with the lowest AGE score of 5.457 and 5.524 respectively. However all methods except DCP and DECOLOR achieved nearly equal score of average gray level error for background estimation (Table 1). For instance in the case of DCP, video sequence ”Bus Stop Morning” achieved the lowest AGE score of 3.164 among all compared methods, its visual result is shown in Figure 1 (d).

4.1.1 Overall Performance Comparison of DCP for Background Estimation

Upon averaging the results from all the 7 categories, DCP achieved an average gray level error to be 8.724 which is minimum among all the compared methods as shown in Figure 5 (a). For fair comparison and evalu-

Table 1 The AGE scores over SBM.net dataset for the six state of the art methods compared with DCP for background subtraction. The best AGE score for each video sequence is shown in blue, and the best average AGE scores for each category is shown in red.

Category	Videos	AGE						
		DCP	RFSA [16]	GRASTA [18]	BRTF [53]	GOSUS [45]	SSGoDec [54]	DECOLOR [55]
Background Motion	Canoe:	6.3250	14.8805	14.9438	14.8798	14.9677	14.9464	13.6732
	Advertisement Board:	2.3378	3.4762	3.4812	3.4640	3.4733	3.4742	3.6604
	Fall:	19.0737	24.3364	24.6026	24.4283	24.5935	24.5702	24.8117
	Fountain 01:	9.6775	5.7150	5.7539	5.7383	5.7750	5.7442	6.2959
	Fountain 02:	14.0579	7.3288	7.0811	7.3307	7.0867	7.0801	6.4137
	Overpass:	6.4089	14.7162	14.7489	14.7183	14.7614	14.7369	8.6909
Average AGE:		9.6468	11.7422	11.7686	11.7599	12.1183	11.5934	11.6340
Basic:	511:	3.5786	5.0972	6.1220	4.9151	5.2681	6.6025	7.5225
	Blurred:	2.1041	4.9735	47.3112	4.9527	105.1528	51.9253	4.7345
	Camouflage FG Objects:	2.5789	4.7951	5.0457	4.7411	4.3364	5.9418	4.4703
	Complex Background :	6.3453	6.8593	6.2202	6.8868	6.1947	6.1828	5.6215
	Hybrid :	4.2021	6.1795	6.5101	5.9201	6.4777	5.8003	6.6420
	IPPR2:	6.8575	6.9256	6.9256	6.9249	6.9256	6.9256	6.9258
	L.SI.01:	4.1119	3.2955	3.3333	3.2895	3.2895	3.3518	2.5187
	Intelligent Room:	5.9152	3.3890	3.4871	3.3546	3.5144	3.4951	3.3934
	Intersection :	2.6911	13.9704	13.9690	13.9752	13.9720	13.9726	13.1152
	MPEG4.40:	3.9292	4.3346	5.6052	4.2712	5.5649	5.6711	3.7329
	PETS2006:	6.5818	4.7506	5.5686	4.7573	5.4968	5.6115	5.5221
	Fluid Highway:	4.3549	12.1362	9.3360	10.1921	9.3345	9.2739	10.1913
	Highway :	4.8638	4.0454	4.1048	4.0381	4.0901	4.0941	4.0762
	Skating :	5.855	26.0429	25.9610	26.1047	26.0922	25.9509	25.7092
	Street Corner at Night:	9.5308	10.2057	10.1120	10.1791	10.0807	10.1170	12.9509
wetSnow :	12.3658	37.6461	37.7272	38.1130	37.7126	37.7054	38.6056	
Average AGE:		5.3666	9.6654	12.3337	9.5385	15.8439	12.6639	9.7332
Intermittent Motion:	AVSS2007:	7.3008	21.3837	21.3776	21.3957	21.3896	21.3746	35.5689
	CaVignal :	13.9885	1.6927	1.7240	1.7131	1.7379	1.7182	1.3504
	Candela m1.10:	8.6512	3.8845	3.8889	3.9102	3.8977	3.9043	5.4697
	LCA.01:	16.8939	15.4821	15.4496	15.4985	15.4312	15.4297	14.6558
	LCA.02:	13.4803	9.9255	6.6146	9.8810	6.2029	7.1204	9.8810
	LMB.01:	9.2338	8.1882	7.3860	8.0478	7.1827	7.6550	11.5584
	LMB.02:	9.5397	8.6324	8.6360	8.6361	8.6307	8.6353	3.6324
	Teknomo:	4.8436	6.7690	6.7382	6.7388	6.7315	6.7312	6.7310
	UCF-traffic:	4.1126	33.0448	33.0449	33.0464	33.0426	33.0432	32.9837
	Utturn:	7.4448	23.4947	23.5190	23.4939	23.5187	23.5163	21.2872
	Bus Station:	8.9723	3.5451	3.5409	3.5513	3.5525	3.5474	6.5359
	Copy Machine:	7.3156	8.1650	8.2640	8.1819	8.2836	8.2483	4.9248
	Office:	16.6488	9.2656	9.1716	9.2710	9.1694	9.2024	3.3454
	Sofa:	4.9927	4.2697	4.2711	4.2637	4.2708	4.2616	4.1817
	Street Corner:	8.9535	7.6411	7.7734	7.6425	7.6832	7.6832	27.5613
Tramstop:	7.1293	2.4173	2.4268	2.4282	2.4483	2.4153	2.4079	
Average AGE:		9.3438	10.4876	10.2392	10.4812	10.2085	10.2804	12.0047
Jitter:	CMU:	8.1714	7.3476	6.9292	7.3197	7.7878	7.6034	6.8975
	L.MC.02:	9.0549	15.7418	13.9334	15.4235	15.4017	15.6302	15.9440
	L.SM.04:	4.5583	3.3464	2.5355	3.0923	3.7768	4.3339	4.1406
	O.MC.02:	12.6371	16.3119	17.3914	16.6375	16.0443	16.4781	12.3657
	O.SM.04:	7.7459	12.0224	12.0262	13.2998	15.6505	13.9053	15.6806
	Badminton:	14.2284	16.9398	17.1787	16.4044	16.6059	14.2486	6.6003
	Boulevard:	11.5450	19.4259	15.4555	16.6356	20.0932	16.9604	23.8209
	Side Walk:	14.9378	24.7621	24.1964	22.8313	16.5027	15.8949	18.4447
	Traffic:	21.3232	7.5524	24.5624	8.6431	7.5449	6.7522	26.5434
	Average AGE:		11.5780	13.7167	14.9121	13.3652	13.2675	12.4230
Very Short:	CUHK Square:	2.8429	5.4994	4.8949	5.8176	5.2220	5.0429	6.2694
	Dynamic Background :	13.7524	7.7233	7.8492	7.5747	7.9276	7.3880	7.3760
	MIT:	3.5838	4.9527	5.7849	4.4991	5.8378	5.2764	4.9524
	Noisy Night :	3.9116	6.1301	5.5040	6.3509	5.3378	5.6906	5.4483
	Toscana:	11.5422	8.7331	6.4773	7.4022	6.8142	6.3869	7.4014
	Town Center :	4.1427	4.4226	4.4247	4.2329	3.8596	3.9657	4.4225
	Two Leave Shop1cor:	10.0183	4.0515	4.0172	4.2124	3.9300	3.8685	4.0503
	Pedestrians:	5.0736	5.0318	4.9441	4.9996	4.9974	4.9682	5.0225
	People In Shade:	6.9680	9.0900	6.5455	10.7783	3.6842	9.3889	10.7812
	SnowFall:	5.2768	32.8871	31.0542	31.2511	31.8320	30.3902	34.2603
Average AGE:		6.7112	8.8522	8.1496	8.7119	7.9443	8.2366	8.9984
Illumination Changes:	Camera Parameter:	6.2206	75.1204	6.1471	6.1126	6.1389	6.1475	45.2837
	Dataset3 Camera1 :	14.5708	23.3046	22.0816	22.5116	22.0816	22.0816	2.8850
	Dataset3 Camera2:	18.7047	6.5041	5.7156	5.8965	5.7156	5.7156	3.7555
	L.LL.01:	7.4329	8.3048	23.6585	23.5775	23.6585	23.6585	22.4594
	L.LL.02:	19.3833	8.4842	7.5423	7.4007	7.5423	7.5423	5.1225
	Cubicle:	11.4636	26.1490	19.4842	31.2116	19.4842	19.4842	13.0519
Average AGE:		12.9627	24.6445	14.1049	16.1184	14.1035	14.1049	15.4263
Very Long:	Bus Stop Morning :	3.1641	5.6652	5.7055	5.6396	5.6739	5.6794	5.7419
	Dataset4 Camera1:	6.7405	3.1857	3.1886	3.1876	3.1794	3.1948	3.1661
	Ped And Storrow Drive:	8.5110	5.5780	5.0913	5.4323	5.3057	5.2445	4.5065
	Ped And Storrow Drive3 :	2.8661	3.5503	3.6693	3.5531	3.6100	3.5598	3.9688
	Terrace :	6.0016	19.9480	18.9514	19.1109	19.0254	19.0258	10.2339
Average AGE:		5.4567	7.5854	7.3212	7.3847	7.3589	7.3409	5.5234
Average AGE of all categories:		8.7237	13.2359	11.9362	11.9229	12.1183	11.5934	11.6340

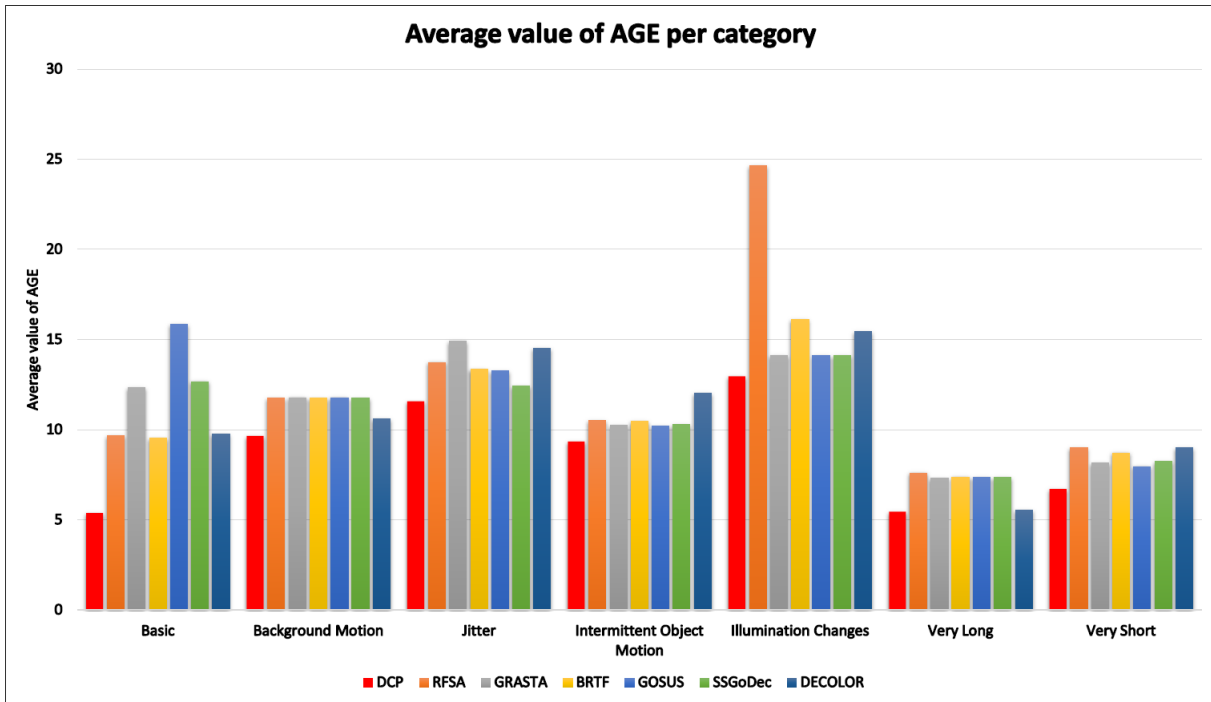


Fig. 4 Performance comparison of each method on the basis of AGE according to each category on SBM.net dataset.

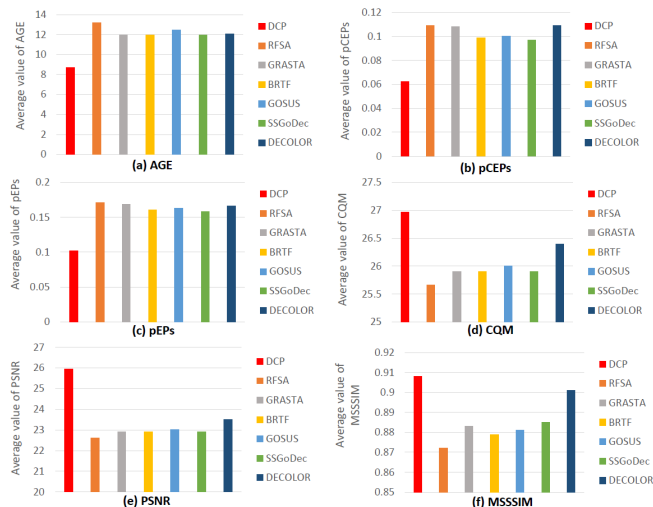


Fig. 5 Average performance comparison of DCP on each metric with 6 state-of-the-art methods on the 7 categories of SBM.net dataset. (a) AGE (b) pCEPs and (c) pEPs, (minimum is best). (d) CQM (e) PSNR (f) MSSSIM, (maximum is best).

ation other than AGE, results of 5 other metrics have also been calculated. In Figure 5 (b), pCEPs which is Percentage of Clustered Error Pixels is minimum for DCP among all compared methods. BRTF, GOSUS and SSGoDec has higher value than DCP. The other three methods GRASTA, RFSA and DECOLOR achieved almost equal and highest score of pCEPs. The

metric pEPs which is basically Percentage of Error Pixels, is aimed to get minimum score for accurate background estimation (Figure 5 (c)). Among all the compared methods only DCP achieved the minimum score while all compared methods showed minimal difference in their pEPs score. In Figure 5 (d) CQM: (Color image Quality Measure), DCP achieved the maximum (best) score for this metric. It can also be seen in the visual results (Figure 3 (d), (e), (f), (g), (h) and (i)) that color quality of some background images extracted by compared methods, is different from input images, ground truths and backgrounds estimated by DCP. Due to this reason all compared methods have different scores of CQM metric. In Figure 5 (e), PSNR: (Peak-Signal-to-Noise-Ratio) and Figure 5 (f) MSSSIM: (MultiScale Structural Similarity Index) should have a highest value for best performance and DCP achieved it efficiently. The proposed DCP algorithm achieved best scores in all mentioned metrics, as compared to the 6 methods.

4.2 Evaluation of Deep Context Prediction (DCP) for Foreground Detection

We have selected 7 categories from CDnet2014 [42] dataset. The results are compared with 6 state-of-the-art methods, including MSSTBM [27], GMM-Zivkovic [56], CP3-Online [25], GMM-Stauffer [39], KDE-Elgammal [11] and RMoG [40] by using implementations of the original

Table 2 Comparison of 6 state of the art methods with the proposed DCP algorithm by using F measure on CDnet2014 dataset. The first highest and the second highest scores for each category is shown in red and blue color respectively.

Categories	MSSTBM [27]	GMM-Zivkovic [56]	CP3-Online [25]	GMM-Stauffer [39]	KDE-ElGammal [11]	RMOG [40]	DCP
Baseline	0.8450	0.8382	0.8856	0.8245	0.9092	0.7848	0.8187
Camera Jitter	0.5073	0.5670	0.5207	0.5969	0.5720	0.7010	0.8376
Shadow	0.8130	0.7232	0.6539	0.7156	0.7660	0.8073	0.7665
Dynamic Background	0.5953	0.6328	0.6111	0.6330	0.5961	0.7352	0.7757
Thermal	0.5103	0.6548	0.7917	0.6621	0.7423	0.4788	0.8212
Intermittent Object Motion	0.4497	0.5325	0.6177	0.5207	0.4088	0.5431	0.5979
Bad Weather	0.6371	0.7406	0.7485	0.7380	0.7571	0.6826	0.8212
Average	0.6225	0.6736	0.7010	0.6771	0.6833	0.6761	0.7620

authors. Foreground detection is compared using Average F measure across all the video sequences within each category. The metrics to calculate F measure are as follows :

$$Re = \frac{T_p}{T_p + F_n}, \quad (12)$$

$$Sp = \frac{T_n}{T_n + F_p}, \quad (13)$$

$$FNR = \frac{F_n}{T_p + F_n}, \quad (14)$$

$$PWC = 100 \times \left(\frac{F_n + F_p}{T_p + F_n + F_p + T_n} \right), \quad (15)$$

$$Pre = \frac{T_p}{T_p + F_p}, \quad \text{and} \quad (16)$$

$$F = \frac{2(Pre \times Re)}{Pre + Re}, \quad (17)$$

where T_p is True positives, T_n is True negatives, F_p is False positives, F_n is False negatives, Re is Recall, Sp is Specificity, FNR is False Negative Rate, PWC Percentage of Wrong Classifications, Pre is Precision and F is F-Measure. Following is the detailed explanation of results on 7 categories of CDnet2014 dataset.

Category: Baseline in CDnet2014 dataset contains 4 video sequences. The average F measure score across all 4 video sequences is shown in Table 2. All the compared methods including DCP achieved more than 0.8 score for this category (Table 2). However KDE-ElGammal successfully got the highest score leaving CP3-Online on second position among all compared methods. Although DCP achieved more than 0.8 F measure score but still it was not able to beat KDE-ElGammal method due to the fact that successive opening and closing on noisy video frames lead to false detection. Visual results are shown in Figure 6 first row.

Category: Camera Jitter also contains 4 video sequences. DCP achieved the highest F measure among

all the compared methods, as shown in Table 2. It is due to the fact that blurry context because of camera jitter is easy to predict by our proposed method for accurate background estimation. Afterwards the binarized thresholded difference of the estimated background and current frame erodes the noisy pixels of background in successive opening and closing operations. This leads us to get accurate foreground detection with less missing pixel values of foreground objects (Figure 6: 3rd row). RMOG also performed well in this category and achieved the second best score among all compared methods.

Category: Shadow contains 6 video sequences. MSSTBM achieved the highest score among all compared methods with RMOG as second best score. This category posed challenge to our proposed method as sometimes shadows got replicated in the context prediction algorithm which generates errors in background estimation as well as foreground detection. In our proposed method the opening and closing of the binarized thresholded difference frame successfully filled the missing values in the foreground detection as shown in the Figure 6: 6th row as compared to all methods. This leads DCP to achieved 3rd best F measure in this category.

Category: Dynamic Background also contains 6 video sequences. DCP achieved the highest averaged F measure among all the compared methods, see Table 2. The homogeneous context in video sequences of this category is a favorable condition for our proposed method. RMOG also performed well and achieved the second best F measure score. The qualitative results are as shown in Figure 6. It can be seen in the visual results that successive opening and closing with a suitable SE removed the noisy pixel values of moving background.

Category: Thermal contains 5 video sequences that have been captured by far-infrared camera. DCP achieved highest averaged F measure score among all compared methods, while CP3-Online is the second best. It is because of the same reason as explained in previous category. The homogeneous context is one of the major key for accurate background estimation of DCP, and it leads to noise-less foreground detection. Figure 6: 7th row shows that all methods including DCP accurately detected foreground object except RMOG which con-

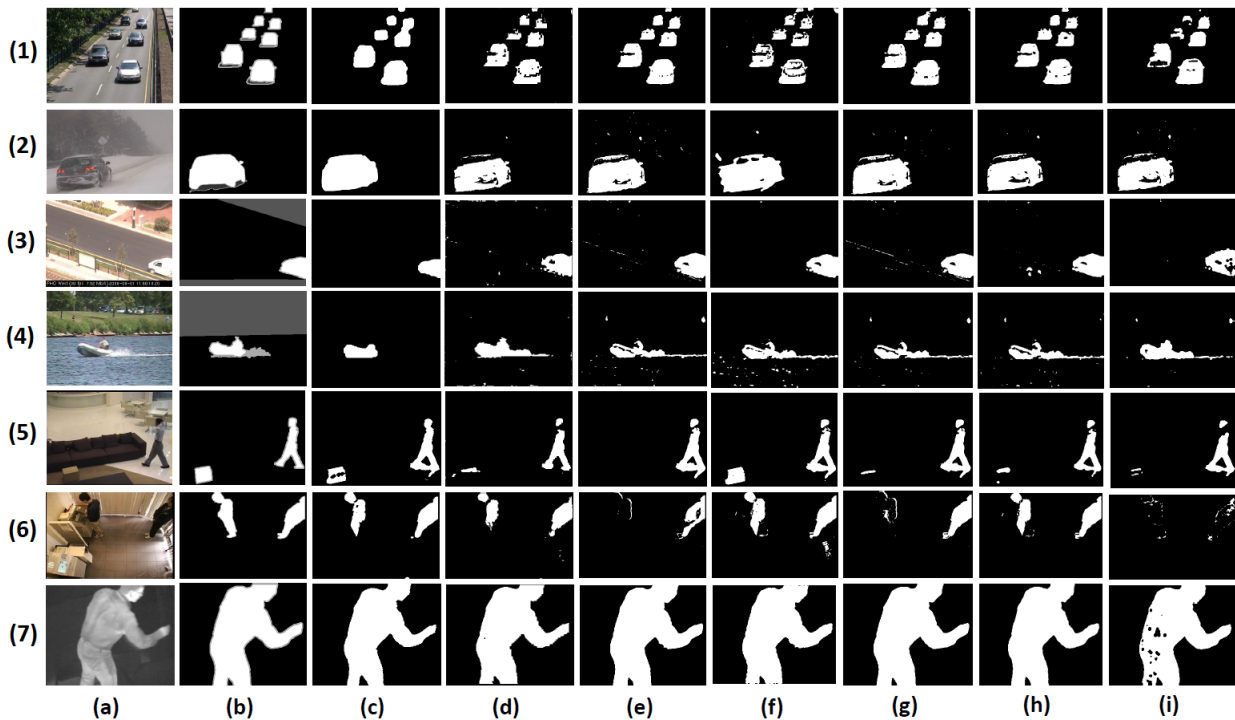


Fig. 6 Qualitative results of the proposed DCP method: (a) Seven images from the input video sequences of Cdnet2014 dataset, (b) Ground truth, (c) Foreground detected by the proposed DCP method, (d) MSSTBM, (e) GMM-Zivkovic, (f) CP3-Online, (g) GMM-Stauffer, (h) KDE-ElGammal, (i) RMOG. From top to bottom: each input sequence is selected from different category: (1) sequence ‘Highway’ from ‘Baseline’, (2) ‘Snowfall’ from ‘Bad Weather’, (3) ‘Boulevard’ from ‘Camera Jitter’, (4) ‘Boats’ from ‘Dynamic Background’, (5) ‘Sofa’ from ‘Intermittent Object Motion’, (6) ‘Copy Machine’ from ‘Shadow’, and (7) ‘Library’ from ‘Thermal’.

tains missing pixel values within detected foreground object.

Category: Intermittent Object Motion contains 6 video sequences with scenarios known for causing ghosting artifacts in the detected motion, i.e., objects move, then stop for a short while, after which they start moving again. DCP achieved the highest average F measure score in this category, while RMOG is the second best among all the compared methods. The main reason behind this is, our proposed approach does not contain any motion-based constraints for moving foreground objects. Since all the compared methods contain constraints on the motion of the foreground objects, which if violated lead to false detection and low F measure score. The visual results in Figure 6: 5th row show that the foreground objects vanish if motion-based constraints are violated.

Category: Bad Weather contains 4 video sequences captured in challenging winter weather conditions, i.e., snow storm, snow on the ground, and fog. DCP achieved highest averaged F measure among all compared methods while KDE-ELGammal is the second best method. This category is another example of homogeneous context in video sequences. It can be seen in the visual results, Figure 6: 2nd row, DCP estimated the almost

accurate foreground object with no unconnected noisy pixels of background as compared to the other methods.

4.2.1 Overall Performance Comparison of DCP for Foreground Detection

Table 2 shows that DCP achieved the highest average F measure score over all categories. CP3-Online is the 2nd best algorithm. GMM-Stauffer, GMM-Zivkovic, KDE-ElGammal and RMOG achieved almost equal F measure with a minimal difference. MSSTBM achieved the lowest score among all the compared methods (Table 2). For better foreground detection the aim of the metrics (defined in (12), (13), (14), (15), and (16)) is to maximize the values of Re, Sp and Precision and minimize the values of FNR and PWC. The proposed DCP algorithm achieved top score in Re and FNR which is 0.809 and 0.191 respectively among all the compared methods. It means that more correct detection and less incorrect detection of foreground objects by our proposed method. Moreover for metrics like PWC, Sp and Precision, DCP achieved 2.671, 0.977 and 0.773 best scores respectively which are higher than most of the methods.

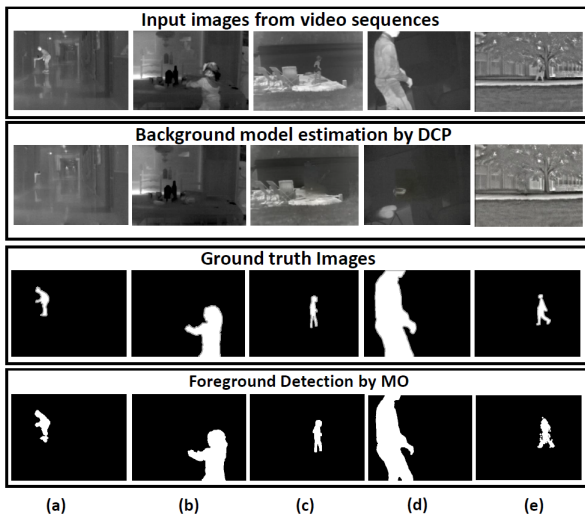


Fig. 7 Estimated background examples from the CDnet2014 dataset : all sequences are from the category "Thermal". (a) Sequence "Corridor". (b) Sequence "Dining Room". (c) Sequence "Lake Side". (d) Sequence "Library". (e) Sequence "Park". In all of these video sequences, DCP estimated an accurate the background which leads to better foreground detection as well.

4.3 Performance of DCP on the basis of Homogeneous Context

As explained in Section 3, our proposed method estimates the background on the basis of context prediction, so in this section we discuss the key aspects of DCP on the type of contexts present in the video sequences containing different scenes specifically for the application of background estimation.

Table 1 shows that for all categories, AGE score is different even for individual videos per category for all the compared methods including DCP. The reason behind that is, the context of every video is different with different kinds of indoor outdoor scenes. Therefore, for compared methods including DCP the average gray level score is different and quite challenging in some cases as well. For convenience, we are targeting the discussion of homogeneous context to few video sequences in SBM.net and CDnet2014 dataset. We have selected 2 categories from CDnet2014 dataset on the basis of their homogeneous context in the video sequences. Category wise discussion is as follows:

Category: Bad Weather is a similar context example from CDnet2014 dataset. Figure 8 shows the visual result of video sequence "blizzard" however other three video sequences are same, "skating", "wetsnow" and "snowfall" from category "Basic" in SBM.net dataset. These video sequences have minimum score of AGE and their visual result are shown in Figure 3 (c): 2nd, 4th and 6th row and Figure 8.

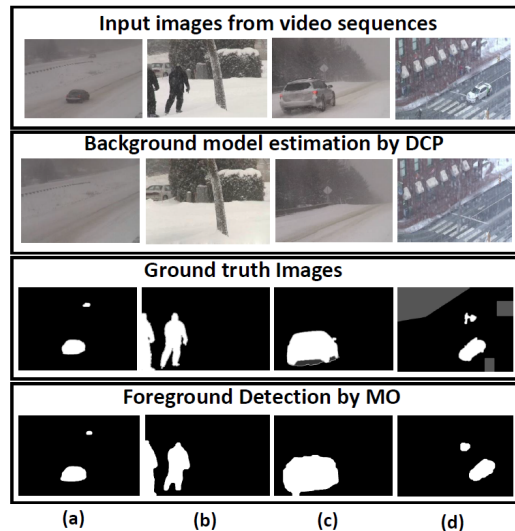


Fig. 8 Estimated background examples from the CDnet2014 dataset: sequences in (a) are from the category 'Bad Weather' named 'Blizzard'. (b) Sequence 'Skating'. (c) Sequence 'Snow-Fall'. (d) Sequence 'WetSnow'. In all of these video sequences, DCP estimated an accurate background which leads to better foreground detection as well.

Category:Thermal is another challenging category in CDnet2014 which includes videos that have been captured by far-infrared cameras. The interesting fact about this category is it includes video sequences with thermal artifacts such as heat stamps, heat reflection on floors, windows, camouflage effects, and a moving object may have the same temperature as the surrounding regions ². It is very favorable environment for DCP for context prediction. The visual results of all 5 video sequences for this category are shown in Figure 7.

4.4 Failure Cases for DCP

Although DCP achieved good performance in most of the cases, still it has some limitations and failure cases. Estimation of complex background structures (Figure 9) and large scale foreground objects is quite challenging. The limitation of the proposed method involves large sized foreground objects to be accurately inpainted. In these cases, the network is not able to properly fill the region in an irregular shape. We used Poisson blending technique to transform center region inpainting context to irregular region one.

² <http://jacarini.dinf.usherbrooke.ca/datasetOverview/>

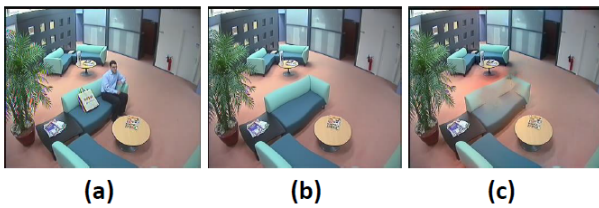


Fig. 9 Estimated background example from the SBM.net dataset: (a) Sequence *Candela m1.10* (b) Ground truth (c) Estimated background by DCP. Table 1 shows that for category ‘Intermittent Motion’ AGE of DCP is maximum than all the compared methods.

5 Conclusion

In this work a unified method ‘Deep Context Prediction’ (DCP) is proposed for background estimation and foreground segmentation using GAN and image inpainting. The proposed method is based on an unsupervised visual feature learning based hybrid GAN for context prediction along with semantic inpainting network for texture optimization. Solution of random region inpainting is also proposed by using center region inpainting and Poisson blending. The proposed DCP algorithm is compared with six existing algorithms for background estimation on SBM.net dataset. The proposed algorithm has outperformed these compared methods with a significant margin. The proposed algorithm is also compared with six foreground segmentation methods on CDnet2014 dataset. On the average, the proposed algorithm has outperformed these algorithms. These experiments demonstrate the effectiveness of the proposed approach compared to the existing algorithms. The proposed algorithm has demonstrated excellent results in bad weather and thermal imaging categories in which most of the existing algorithms suffer from performance degradation.

Acknowledgements This study was supported by the BK21 Plus project (SW Human Resource Development Program for Supporting Smart Life) funded by the Ministry of Education, School of Computer Science and Engineering, Kyungpook National University, Korea (21A20131600005).

References

1. Afifi M, Hussain KF (2015) Mpb: A modified poisson blending technique. *Computational Visual Media* 1(4):331–341
2. Bengio Y, et al (2009) Learning deep architectures for ai. *Foundations and trends® in Machine Learning* 2(1):1–127
3. Bouwmans T, Zahzah EH (2014) Robust pca via principal component pursuit: A review for a comparative evaluation in video surveillance. *Computer Vision and Image Understanding* 122:22–34
4. Bouwmans T, Maddalena L, Petrosino A (2017) Scene background initialization: a taxonomy. *Pattern Recognition Letters* 96:3–11
5. Braham M, Van Droogenbroeck M (2016) Deep background subtraction with scene-specific convolutional neural networks. In: *Systems, Signals and Image Processing (IWSSIP), 2016 International Conference on, IEEE*, pp 1–4
6. Candès EJ, Li X, Ma Y, Wright J (2011) Robust principal component analysis? *Journal of the ACM (JACM)* 58(3):11
7. Cao X, Yang L, Guo X (2016) Total variation regularized rpca for irregularly moving object detection under dynamic background. *IEEE transactions on cybernetics* 46(4):1014–1027
8. Chen M, Wei X, Yang Q, Li Q, Wang G, Yang MH (2017) Spatiotemporal gmm for background subtraction with superpixel hierarchy. *IEEE transactions on pattern analysis and machine intelligence*
9. Colombari A, Cristani M, Murino V, Fusiello A (2005) Exemplar-based background model initialization. In: *Proceedings of the third ACM international workshop on Video surveillance & sensor networks*, ACM, pp 29–36
10. Deng J, Dong W, Socher R, Li LJ, Li K, Fei-Fei L (2009) ImageNet: A Large-Scale Hierarchical Image Database. In: *CVPR09*
11. Elgammal A, Harwood D, Davis L (2000) Non-parametric model for background subtraction. In: *European conference on computer vision*, Springer, pp 751–767
12. Erichson NB, Donovan C (2016) Randomized low-rank dynamic mode decomposition for motion detection. *Computer Vision and Image Understanding* 146:40–50
13. Gao Z, Cheong LF, Wang YX (2014) Block-sparse RPCA for salient motion detection. *IEEE T-PAMI* 36(10):1975–1987
14. Girshick R, Donahue J, Darrell T, Malik J (2016) Region-based convolutional networks for accurate object detection and segmentation. *IEEE transactions on pattern analysis and machine intelligence* 38(1):142–158
15. Goodfellow I, Pouget-Abadie J, Mirza M, Xu B, Warde-Farley D, Ozair S, Courville A, Bengio Y (2014) Generative adversarial nets. In: *Advances in neural information processing systems*, pp 2672–2680
16. Guo X, Wang X, Yang L, Cao X, Ma Y (2014) Robust foreground detection using smoothness and arbitrariness constraints. In: *European Conference*

- on Computer Vision, Springer, pp 535–550
17. Haines TS, Xiang T (2014) Background subtraction with dirichletprocess mixture models. *IEEE transactions on pattern analysis and machine intelligence* 36(4):670–683
 18. He J, Balzano L, Szlam A (2012) Incremental gradient on the grassmannian for online foreground and background separation in subsampled video. In: *Computer Vision and Pattern Recognition (CVPR), 2012 IEEE Conference on*, IEEE, pp 1568–1575
 19. Hinton GE, Salakhutdinov RR (2006) Reducing the dimensionality of data with neural networks. *science* 313(5786):504–507
 20. Javed S, Oh SH, Bouwmans T, Jung SK (2015) Robust background subtraction to global illumination changes via multiple features-based online robust principal components analysis with markov random field. *Journal of Electronic Imaging* 24(4):043011
 21. Javed S, Jung SK, Mahmood A, Bouwmans T (2016) Motion-aware graph regularized rpca for background modeling of complex scenes. In: *Pattern Recognition (ICPR), 2016 23rd International Conference on*, IEEE, pp 120–125
 22. Javed S, Mahmood A, Bouwmans T, Jung SK (2017) Background-foreground modeling based on spatiotemporal sparse subspace clustering. *IEEE Transactions on Image Processing* 26(12):5840–5854
 23. Javed S, Mahmood A, Bouwmans T, Jung SK (2017) Background-Foreground Modeling Based on Spatiotemporal Sparse Subspace Clustering. *IEEE T-IP*
 24. Krizhevsky A, Sutskever I, Hinton GE (2012) Imagenet classification with deep convolutional neural networks. In: *Advances in neural information processing systems*, pp 1097–1105
 25. Liang D, Hashimoto M, Iwata K, Zhao X, et al (2015) Co-occurrence probability-based pixel pairs background model for robust object detection in dynamic scenes. *Pattern Recognition* 48(4):1374–1390
 26. Liu C, et al (2009) Beyond pixels: exploring new representations and applications for motion analysis. PhD thesis, Massachusetts Institute of Technology
 27. Lu X (2014) A multiscale spatio-temporal background model for motion detection. In: *Image Processing (ICIP), 2014 IEEE International Conference on*, IEEE, pp 3268–3271
 28. Maddalena L, Petrosino A (2015) Towards benchmarking scene background initialization. In: *International Conference on Image Analysis and Processing*, Springer, pp 469–476
 29. Nakashima Y, Babaguchi N, Fan J (2011) Automatic generation of privacy-protected videos using background estimation. In: *Multimedia and Expo (ICME), 2011 IEEE International Conference on*, IEEE, pp 1–6
 30. Ortego D, SanMiguel JC, Martínez JM (2016) Rejection based multipath reconstruction for background estimation in video sequences with stationary objects. *Computer vision and image understanding* 147:23–37
 31. Park D, Byun H (2013) A unified approach to background adaptation and initialization in public scenes. *Pattern Recognition* 46(7):1985–1997
 32. Pathak D, Krahenbuhl P, Donahue J, Darrell T, Efros AA (2016) Context encoders: Feature learning by inpainting. In: *Proceedings of the IEEE Conference on Computer Vision and Pattern Recognition*, pp 2536–2544
 33. Pérez P, Gangnet M, Blake A (2003) Poisson image editing. *ACM Transactions on graphics (TOG)* 22(3):313–318
 34. Ren S, He K, Girshick R, Sun J (2015) Faster r-cnn: Towards real-time object detection with region proposal networks. In: *Advances in neural information processing systems*, pp 91–99
 35. Shimada A, Nagahara H, Taniguchi Ri (2013) Background modeling based on bidirectional analysis. In: *Computer Vision and Pattern Recognition (CVPR), 2013 IEEE Conference on*, IEEE, pp 1979–1986
 36. Simonyan K, Zisserman A (2014) Very deep convolutional networks for large-scale image recognition. *arXiv preprint arXiv:14091556*
 37. Sobral A, Zahzah Eh (2017) Matrix and tensor completion algorithms for background model initialization: A comparative evaluation. *Pattern Recognition Letters* 96:22–33
 38. Sobral A, Bouwmans T, Zahzah EH (2015) Comparison of matrix completion algorithms for background initialization in videos. In: *International Conference on Image Analysis and Processing*, Springer, pp 510–518
 39. Stauffer C, Grimson WEL (1999) Adaptive background mixture models for real-time tracking. In: *Computer Vision and Pattern Recognition, 1999. IEEE Computer Society Conference on*, IEEE, vol 2, pp 246–252
 40. Varadarajan S, Miller P, Zhou H (2013) Spatial mixture of gaussians for dynamic background modelling. In: *Advanced Video and Signal Based Surveillance (AVSS), 2013 10th IEEE International Conference on*, IEEE, pp 63–68

41. Viola P, Jones M (2001) Rapid object detection using a boosted cascade of simple features. In: *Computer Vision and Pattern Recognition, 2001. CVPR 2001. Proceedings of the 2001 IEEE Computer Society Conference on, IEEE*, vol 1, pp I–I
42. Wang Y, Jodoin PM, Porikli F, Konrad J, Benezeth Y, Ishwar P (2014) Cdnet 2014: An expanded change detection benchmark dataset. In: *Computer Vision and Pattern Recognition Workshops (CVPRW), 2014 IEEE Conference on, IEEE*, pp 393–400
43. Wang Y, Luo Z, Jodoin PM (2017) Interactive deep learning method for segmenting moving objects. *Pattern Recognition Letters* 96:66–75
44. Wright J, Ganesh A, Rao S, Peng Y, Ma Y (2009) Robust principal component analysis: Exact recovery of corrupted low-rank matrices via convex optimization. In: *Advances in neural information processing systems*, pp 2080–2088
45. Xu J, Ithapu V, Mukherjee L, Rehg J, Singh V (2013) Gosus: Grassmannian online subspace updates with structured-sparsity. In: *ICCV*
46. Xu J, Ithapu VK, Mukherjee L, Rehg JM, Singh V (2013) Gosus: Grassmannian online subspace updates with structured-sparsity. In: *Computer Vision (ICCV), 2013 IEEE International Conference on, IEEE*, pp 3376–3383
47. Xu X, Huang TS (2008) A loopy belief propagation approach for robust background estimation. In: *Computer Vision and Pattern Recognition, 2008. CVPR 2008. IEEE Conference on, IEEE*, pp 1–7
48. Yang C, Lu X, Lin Z, Shechtman E, Wang O, Li H (2016) High-resolution image inpainting using multi-scale neural patch synthesis. *arXiv preprint arXiv:161109969*
49. Ye X, Yang J, Sun X, Li K, Hou C, Wang Y (2015) Foreground–background separation from video clips via motion-assisted matrix restoration. *IEEE Transactions on Circuits and Systems for Video Technology* 25(11):1721–1734
50. Zhang T, Liu S, Xu C, Lu H (2013) Mining semantic context information for intelligent video surveillance of traffic scenes. *IEEE transactions on industrial informatics* 9(1):149–160
51. Zhang T, Liu S, Ahuja N, Yang MH, Ghanem B (2015) Robust visual tracking via consistent low-rank sparse learning. *International Journal of Computer Vision* 111(2):171–190
52. Zhang Y, Li X, Zhang Z, Wu F, Zhao L (2015) Deep learning driven blockwise moving object detection with binary scene modeling. *Neurocomputing* 168:454–463
53. Zhao Q, Zhou G, Zhang L, Cichocki A, Amari SI (2016) Bayesian robust tensor factorization for incomplete multiway data. *IEEE transactions on neural networks and learning systems* 27(4):736–748
54. Zhou T, Tao D (2011) Godec: Randomized low-rank and sparse matrix decomposition in noisy case. In: *ICML, Omnipress*
55. Zhou X, Yang C, Yu W (2013) Moving object detection by detecting contiguous outliers in the low-rank representation. *IEEE T-PAMI* 35(3):597–610
56. Zivkovic Z (2004) Improved adaptive gaussian mixture model for background subtraction. In: *Pattern Recognition, 2004. ICPR 2004. Proceedings of the 17th International Conference on, IEEE*, vol 2, pp 28–31

Maryam Sultana is a PhD student at Virtual Reality Lab, School of Computer Science and Engineering, Kyungpook National University Republic of Korea. She received her M.Sc. and M.Phil. degrees in electronics from Quaid-i-Azam university Pakistan in 2013 and 2016, respectively. Her research interests include background modeling, foreground object detection and generative adversarial networks.

Arif Mahmood received the masters and Ph.D. degrees in computer science from the Lahore University of Management Sciences, Lahore, Pakistan, in 2003 and 2011, respectively. He was a Research Assistant Professor with the School of Computer Science and Software Engineering, The University of Western Australia (UWA), where he was involved in hyper-spectral object recognition and action recognition using depth images. He was a Research Assistant Professor with the School of Mathematics and Statistics, UWA, where he was involved in the characterizing structure of complex networks using sparse subspace clustering. He is currently a Post-Doctoral Researcher with the Department of Computer Science and Engineering, Qatar University, Doha. He has performed research in data clustering, classification, action, and object recognition. His major research interests are in computer vision and pattern recognition, action detection and person segmentation in crowded environments, and background-foreground modeling in complex scenes.

Sajid Javed is currently a Post-doctoral research fellow in the Department of Computer Science, University of Warwick, United Kingdom. He obtained his Bs.c (hons) degree in Computer Science from University of Hertfordshire, UK, in 2010. He joined the Virtual Reality Laboratory of Kyungpook National University, Republic of Korea, in 2012 where he completed his com-

bined Master's and Doctoral degrees in Computer Science. His research interests include background modeling and foreground object detection, robust principal component analysis, matrix completion, and subspace clustering.

Soon Ki Jung is a professor in the School of Computer Science and Engineering at Kyungpook National University, Republic of Korea. He received his MS and PhD degrees in computer science from Korea Advanced Institute of Science and Technology (KAIST), Korea, in 1992 and 1997, respectively. He has been a visiting professor at University of Southern California, USA, in 2009. He has been an active executive board member of Human Computer Interaction, Computer Graphics, and Multimedia societies in Korea. Since 2007, he has also served as executive board member of IDIS Inc. His research areas include a broad range of computer vision, computer graphics, and virtual reality topics.